Image Resolution Enhancement Using Dual-tree Complex Wavelet Transform

Turgay Celik and Tardi Tjahjadi

Abstract

In this letter, a complex wavelet-domain image resolution enhancement algorithm based on the estimation of wavelet coefficients is proposed. The method uses forward and inverse dual-tree complex wavelet transform (DT-CWT) to construct the high-resolution (HR) image from the given low-resolution (LR) image. The HR image is reconstructed from the LR image together with a set of wavelet coefficients using the inverse dual-tree complex wavelet transform (IDT-CWT). The set of wavelet coefficients is estimated from the DT-CWT decomposition of the rough estimation of the HR image. Results are presented and discussed on very high-resolution QuickBird data, through comparisons between state-of-the-art resolution enhancement methods.

Index Terms

Resolution enhancement, image interpolation, dual-tree complex wavelet transform, discrete wavelet transform, satellite image.

I. Introduction

Image resolution enhancement is a usable preprocess for many satellite image processing applications, such as vehicle recognition, bridge recognition, and building recognition to name a few. Image resolution enhancement techniques can be categorized into two major classes according to the domain they are applied in: 1) image-domain; and 2) transform-domain. The techniques in image-domain use the statistical and geometric data directly extracted from the input image itself [1], [2], while transform-domain techniques use transformations such as decimated discrete wavelet transform to achieve the image resolution enhancement [3]–[6].

The decimated discrete wavelet transform (DWT) has been widely used for performing image resolution enhancement [3]–[5]. A common assumption of DWT-based image resolution enhancement is that the low-resolution (LR) image is the low-pass filtered subband of the wavelet-transformed high-resolution (HR) image. This type of approach requires the estimationof wavelet coefficients in subbands containing high-pass spatial frequency information in order to estimate the HR image from the LR image.

In order to estimate the high-pass spatial frequency information, many different approaches have been introduced. In [3], [4], only the high-pass coefficients with significant magnitudes are estimated as the evolution of the wavelet coefficients among the scales. The performance is mainly affected from the fact that the signs of estimated coefficients are copied directly from parent coefficients without any attempt being made to estimate the actual signs. This is contradictory to the fact that there is very little correlation between the signs of the parent coefficients and their descendants. As a result, the signs of the coefficients estimated using extreme evolution techniques cannot be relied upon. Hidden Markov tree (HMT) based method in [5] models the unknown wavelet coefficients as belonging to mixed Gaussian distributions which are symmetrical about the zero mean. HMT models are used to determine the most probable state for the coefficients to be estimated. The performance also suffers mainly from the sign changes between the scales.

The decimated DWT is not shift-invariant and, as a result, suppression of wavelet coefficients introduces artifacts into the image which manifests as ringing in the neighbourhood of discontinuities [6]. In order to combat this drawback in DWT-based

Manuscript received 21 0ctober, 2009; revised 10 December, 2009; accepted 27 December, 2009. This work was supported by the Warwick University Vice Chancellor Scholarship.

Turgay Celik and Tardi Tjahjadi are with the School of Engineering, University of Warwick Gibbet Hill Road, Coventry, CV4 7AL, United Kingdom. e-mail: Turgay Celik (t.celik@warwick.ac.uk; celikturgay@gmail.com), Tardi Tjahjadi (t.tjahjadi@warwick.ac.uk).

image resolution enhancement, cycle-spinning methodology was adopted in [6]. The perceptual and objective quality of the resolution enhanced images by their method compare favourably with recent methods [3], [5] in the field.

Dual-tree complex wavelet transform (DT-CWT) is introduced to alleviate the drawbacks caused by the decimated DWT [7]. It is shift invariant and has improved directional resolution when compared with that of the decimated DWT. Such features make it suitable for image resolution enhancement. In this letter, a complex wavelet-domain image resolution enhancement algorithm based on the estimation of wavelet coefficients at high resolution scales is proposed. The initial estimate of the HR image is constructed by applying cycle-spinning methodology [6] in DT-CWT domain. It is then decomposed using the one-level DT-CWT to create a set of high-pass coefficients at the same spatial resolution of the LR image. The high-pass coefficients together with the LR image are used to reconstruct the HR image using inverse DT-CWT.

The letter is organized as follows. Section II gives a brief review of the DT-CWT. Section III describes the proposed DT-CWT domain satellite image resolution enhancement algorithm. Section IV provides some experimental results of the proposed approach and comparisons with the approaches in [1], [2], [4], and [6]. Section V concludes the letter.

II. Dual-tree Complex Wavelet Transform

The dual-tree complex wavelet transform is a combination of two real-valued decimated discrete wavelet transforms. The ordinary decimated DWT is shift variant due to the decimation operation exploited in the transform. As a result, a small shift in the input signal can result in a very different set of wavelet coefficients. For that, Kingsbury [7] introduced a new kind of wavelet transform, called the dual-tree complex wavelet transform which exhibits shift invariant property and improves directional resolution when compared with that of the decimated DWT.

The DT-CWT also yields perfect reconstruction by using two parallel decimated trees with real-valued coefficients generated at each tree. The one-dimensional (1-D) DT-CWT decomposes the input signal $f(x)$ by expressing it in terms of a complex shifted and dilated mother wavelet $\Psi(x)$ and scaling function $\Phi(x)$, i.e.,

$$f(x) = \sum_{l \in Z} s_{j_0,l} \Phi_{j_0,l}(x) + \sum_{j \geq j_0} \sum_{l \in Z} c_{j,l} \Psi_{j,l}(x), \tag{1}$$

where Z is the set of natural numbers, j and l refer to the index of shifts and dilations respectively, $s_{j_0,l}$ is the scaling coefficient and $c_{j,l}$ is the complex wavelet coefficient with $\Phi_{j_0,l}(x) = \Phi^r_{j_0,l}(x) + \sqrt{-1}\Phi^i_{j_0,l}(x)$ and $\Psi_{j,l}(x) = \Psi^r_{j,l}(x) + \sqrt{-1}\Psi^i_{j,l}(x)$, where the superscripts r and i denote the real part and the imaginary part, respectively. In the 1-D DT-CWT case, the set $\{\Phi^r_{j_0,l}, \Phi^i_{j_0,l}, \Psi^r_{j_0,l}, \Psi^i_{j_0,l}\}$ forms a tight wavelet frame with double redundancy. The real and imaginary parts of the 1-D DT-CWT are computed using separate filter banks with filters h_0 and h_1 for the real part, and g_0 and g_1 for the imaginary part [7].

Similar to the 1-D DT-CWT, the two-dimensional (2-D) DT-CWT decomposes a 2-D image $f(x, y)$ through a series of dilations and translations of a complex scaling function and six complex wavelet functions $\Psi^\theta_{j,l}$, i.e.,

$$f(x,y) = \sum_{l \in Z^2} s_{j_0,l} \Phi_{j_0,l}(x,y) + \sum_{\theta \in \Theta} \sum_{j \geq j_0} \sum_{l \in Z^2} c^\theta_{j,l} \Psi^\theta_{j,l}(x,y). \tag{2}$$

where $\theta \in \Theta = \{\pm 15^\circ, \pm 45^\circ, \pm 75^\circ\}$ provides the directionality of the complex wavelet function. In other words, the decomposition of $f(x, y)$ by exploiting the DT-CWT produces one complex-valued low-pass subband and six complex-valued high-pass subbands at each level of decomposition, where each high-pass subband corresponds to one unique direction θ.

III. Proposed Method

Let us consider the unknown $2H \times 2W$ HR image $\mathbf{X}_{\mathrm{H}}$ and the known $H \times W$ LR image $\mathbf{X}_{\mathrm{L}}$. The aim of the enhancement is to generate an estimate HR image $\hat{\mathbf{X}}_{\mathrm{H}}$ of the unknown HR image $\mathbf{X}_{\mathrm{H}}$ using the known LR image $\mathbf{X}_{\mathrm{L}}$. Let us further assume that the one-level DT-CWT decomposition of an $2H \times 2W$ image $\mathbf{X}$ results in a matrix of DT-CWT$(\mathbf{X}) = [\mathbf{LP_X}\ \mathbf{HP_X}]$, and inverse DT-CWT (IDT-CWT) of $[\mathbf{LP_X}\ \mathbf{HP_X}]$ reconstructs the signal $\mathbf{X}$ perfectly, i.e., IDT-CWT$([\mathbf{LP_X}\ \mathbf{HP_X}]) = \mathbf{X}$. The $\mathbf{LP_X}$ is a matrix of size $H \times W$ which is the complex-valued low-pass subband resulting from the one-level DT-CWT decomposition of image $\mathbf{X}$, and $\mathbf{HP_X}$ is a matrix of size $H \times W \times 6$ which is the collection of all six complex-valued high-pass subbands resulting from the one-level DT-CWT decomposition of image $\mathbf{X}$.

(a) (b) (c)

Fig. 1. Reference high-resolution test image and its low-resolution versions obtained by first low-pass filtering and then down-sampling by a sampling factor in both spatial dimensions: (a) Input high-resolution reference image; (b) Low-resolution version of (a) with a sampling factor 2; and (c) Low-resolution version of (a) with a sampling factor 4.

For a given LR image $\mathbf{X}_{\mathrm{L}}$, the proposed resolution enhancement method is made up of the following four main steps: 1) generate the initial estimate ($\mathbf{Y}$) of the HR image; 2) decompose the $\mathbf{Y}$ using one-level DT-CWT to create low-pass and high-pass matrix structure $[\mathbf{LP_Y}\ \mathbf{HP_Y}]$; 3) formulate a matrix structure $[\mathbf{X}_{\mathrm{L}}\ \mathbf{HP_Y}]$ using $[\mathbf{LP_Y}\ \mathbf{HP_Y}]$ and the input LR image $\mathbf{X}_{\mathrm{L}}$; and 4) generate of the HR image by employing the IDT-CWT on $[\mathbf{X}_{\mathrm{L}}\ \mathbf{HP_Y}]$.

The first step employs the cycle-spinning algorithm [6] in DT-CWT domain to create an initial estimate $\mathbf{Y}$ of the unknown HR image.

The second step is the estimation of the high-pass coefficients for the input LR signal $\mathbf{X}_{\mathrm{L}}$. The initial estimate $\mathbf{Y}$ is decomposed using the one-level DT-CWT to create one complex-valued low-pass subband and six complex-valued high-pass subbands with the same spatial resolution as that of $\mathbf{X}_{\mathrm{L}}$, i.e., DT-CWT $(\mathbf{Y}) = [\mathbf{LP_Y}\ \mathbf{HP_Y}]$.

In the final step, the input LR image together with the complex-valued high-pass subbands $\mathbf{HP_Y}$ extracted from the one-level DT-CWT decomposition of $\mathbf{Y}$ are used to create the HR image by employing inverse DT-CWT, i.e.,

$$\hat{\mathbf{X}}_{\mathrm{H}} = \text{IDT-CWT}\left([\mathbf{X}_{\mathrm{L}}\ \mathbf{HP_Y}]\right). \tag{3}$$

IV. Experimental Results

In the experiments, the natural colour (R, G, and B), 60 centimeter (2 foot) high-resolution QuickBird satellite image data is used. The QuickBird data was acquired over Wall Street and the southern tip of Manhattan on April 24, 2009. A test image of size 256×512 pixel at the resolution of 60 cm are cropped from the raw image as shown in Fig. 1 (a), and is used as the reference image. In order to obtain a performance metric in addition to visual assessment of the results using different resolution enhancement methods, we take a 256×512 image, $\mathbf{X}_{\mathrm{H}}$, filter it with 3×3 averaging (low-pass) filter, and down-sample it to obtain two available LR images $\mathbf{X}_{\mathrm{L}}^{(2)}$ and $\mathbf{X}_{\mathrm{L}}^{(4)}$ of sizes 128×256 and 64×128 pixels, respectively. The available LR images are shown in Fig. 1 (b) and 1 (c). The superscripts 2 and 4 denote the down-sample factor. The resolution enhancement methods are applied on LR images $\mathbf{X}_{\mathrm{L}}^{(2)}$ and $\mathbf{X}_{\mathrm{L}}^{(4)}$ to reconstruct an estimate $\hat{\mathbf{X}}_{\mathrm{H}}$ of the known HR image $\mathbf{X}_{\mathrm{H}}$. The original HR image $\mathbf{X}_{\mathrm{H}}$ and the reconstructed HR image $\hat{\mathbf{X}}_{\mathrm{H}}$ are then compared qualitatively and quantitatively. In this letter, images consisting of three spectral bands that correspond to R, G and B channels in natural colour image representation, i.e., $\mathbf{X}_{\mathrm{H}} = \left\{\mathbf{X}_{\mathrm{H}}^{(R)}, \mathbf{X}_{\mathrm{H}}^{(G)}, \mathbf{X}_{\mathrm{H}}^{(B)}\right\}$, $\mathbf{X}_{\mathrm{L}} = \left\{\mathbf{X}_{\mathrm{L}}^{(R)}, \mathbf{X}_{\mathrm{L}}^{(G)}, \mathbf{X}_{\mathrm{L}}^{(B)}\right\}$, are used and resolution enhancement methods are applied to each spectral band of LR image $\mathbf{X}_{\mathrm{L}}$ independently to reconstruct an estimate of the reference image.

The quality of the resolution enhanced images is estimated using several metrics from the remote sensing community. Let the reference HR image $\mathbf{X}_{\mathrm{H}}$ and reconstructed HR image $\hat{\mathbf{X}}_{\mathrm{H}}$ be of size $H \times W$ pixels and consist of three spectral bands, i.e., R, G, and B. The following quantitative metrics are used to compare $\mathbf{X}_{\mathrm{H}}$ and $\hat{\mathbf{X}}_{\mathrm{H}}$:

1) *Spectral Angle Mapper* (SAM) [8]: the average change in angle of all spectral vectors, defined as

$$\text{SAM} = \frac{1}{HW}\sum_{x,y}\arccos\left(\frac{\langle \mathbf{v}(x,y), \hat{\mathbf{v}}(x,y)\rangle}{||\mathbf{v}(x,y)||_2||\hat{\mathbf{v}}(x,y)||_2}\right),$$

where (x, y) is spatial pixel coordinate, $\mathbf{v}(x,y) = \left[v^{(1)}(x,y), v^{(2)}(x,y), v^{(3)}(x,y)\right] = \left[\mathbf{X}_{\mathrm{H}}^{(R)}(x,y), \mathbf{X}_{\mathrm{H}}^{(G)}(x,y), \mathbf{X}_{\mathrm{H}}^{(B)}(x,y)\right]$ denotes the spectral vector of the pixel (x, y) in the reference image, and $\hat{\mathbf{v}}(x,y) = \left[\hat{v}^{(1)}(x,y), \hat{v}^{(2)}(x,y), \hat{v}^{(3)}(x,y)\right] = \left[\hat{\mathbf{X}}_{\mathrm{H}}^{(R)}(x,y), \hat{\mathbf{X}}_{\mathrm{H}}^{(G)}(x,y), \hat{\mathbf{X}}_{\mathrm{H}}^{(B)}(x,y)\right]$ denotes the vector obtained after

resolution enhancement. The SAM value measures the difference in spectral content between corresponding bands of the reference and resolution enhanced images, and should be as close to 0 as possible.

2) *Spectral Information Divergence* (SID) [9]: derived from the concept of divergence arising in information theory and can be used to measure spectral similarity. SID views each pixel spectrum as a random variable and then measures the discrepancy of probabilistic behaviours between two spectra. SID is computed as

$$\begin{aligned}\text{SID} = \sum_{x,y}\sum_{i=1}^{N} & v_n^{(i)}(x,y)\log\left(v_n^{(i)}(x,y)/\hat{v}_n^{(i)}(x,y)\right) \\ & +\hat{v}_n^{(i)}(x,y)\log\left(\hat{v}_n^{(i)}(x,y)/v_n^{(i)}(x,y)\right),\end{aligned}$$

where N is the number of spectral bands, i.e., $N = 3$, $v_n^{(i)}(x,y) = v^{(i)}(x,y)/\sum_{j=1}^{N} v^{(j)}(x,y)$, and $\hat{v}_n^{(i)}(x,y) = \hat{v}^{(i)}(x,y)/\sum_{j=1}^{N}\hat{v}^{(j)}(x,y)$. The SID value should be as close to 0 as possible.

3) *Quality Index Q4* (Q4) [10]: obtained through the use of correlation coefficient between hypercomplex numbers that represent spectral vectors. Q4 is made up of different components (factors) to take into account of the correlation: the mean of each spectral band; the intra-band local variance; and the spectral angle. The highest value of Q4 is 1, which is obtained if and only if the resolution enhanced image is equal to the reference image.

4) *Root Mean Square Error* (RMSE): the root mean square error between the reference image and the resolution enhanced image, i.e.,

$$\text{RMSE} = \sqrt{\frac{1}{N}\sum_{i=1}^{N}\Delta\left(\mathbf{X}_{\text{H}}^{(i)},\hat{\mathbf{X}}_{\text{H}}^{(i)}\right)^2},$$

where

$$\Delta\left(\mathbf{X}_{\text{H}}^{(i)},\hat{\mathbf{X}}_{\text{H}}^{(i)}\right) = \sqrt{\frac{1}{HW}\sum_{x,y}\left(\mathbf{X}_{\text{H}}^{(i)}(x,y) - \hat{\mathbf{X}}_{\text{H}}^{(i)}(x,y)\right)^2}.$$

The RMSE value should be as close to 0 as possible.

5) *Relative Dimensionless Global Error* (ERGAS) [11]: the normalized version of the root mean square error designed to calculate the spectral distortion between the reference image and resolution enhanced image, i.e.,

$$\text{ERGAS} = 100\frac{h}{l}\sqrt{\frac{1}{N}\sum_{i=1}^{N}\Delta\left(\mathbf{X}_{\text{H}}^{(i)},\hat{\mathbf{X}}_{\text{H}}^{(i)}\right)^2/M_i^2},$$

where h/l is the ratio between the pixel sizes of the reference HR image and the LR image, and M_i is the mean radiance of i^{th} spectral band in the reference image. The ERGAS should be as close to 0 as possible.

6) *Correlation Coefficient* (CC): the correlation between each band of the reference image and the resolution enhanced image, i.e.,

$$\text{CC} = \frac{1}{N}\sum_{i=1}^{N}\frac{\sum_{x,y}\left(v^{(i)}(x,y) - \bar{v}^{(i)}\right)\left(\hat{v}^{(i)}(x,y) - \bar{\hat{v}}^{(i)}\right)}{\sqrt{\sum_{x,y}\left(v^{(i)}(x,y) - \bar{v}^{(i)}\right)^2\sum_{x,y}\left(\hat{v}^{(i)}(x,y) - \bar{\hat{v}}^{(i)}\right)^2}},$$

where $\bar{v}^{(i)}$ and $\bar{\hat{v}}^{(i)}$ are the mean values of the corresponding spectral band. The CC value should be as close to 1 as possible.

Experiments are conducted to compare the performance of the proposed approach with that of recently proposed methods in [1], [2], [4], and [6]. We used the authors' implementations for the methods in [1] and [2], and we implemented the methods of [4], and [6].

In the first experiment, we test the performance of different methods on enhancing resolution of the input LR image by a factor 2 in both spatial dimensions. For this, Fig. 1 (a) and Fig. 1 (b) are used as the reference HR image and the input LR image, respectively. Different resolution enhancement methods are applied to Fig. 1 (b) to estimate the reference HR image as shown Fig. 1 (a). Fig. 2 show sub-images cropped from the results of different resolution enhancement methods. The spectral distortions on the enhanced images can be noticed. It can be observed that wavelet-domain methods achieve better visual quality than that of the spatial-domain methods. To evaluate the spectral quality quantitatively, the aforementioned metrics are

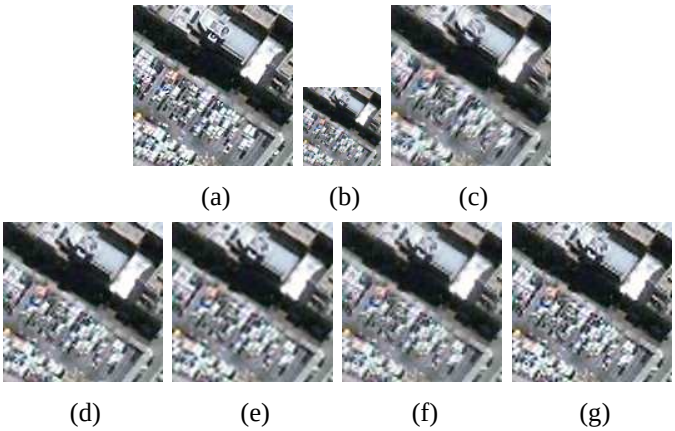

Fig. 2. Results of spatial resolution enhancement with a factor of 2 in both spatial dimensions: (a) Reference HR image; (b) Input LR image; (c) Resolution enhanced image using [1]; (d) Resolution enhanced image using [2]; (e) Resolution enhanced image using [4]; (f) Resolution enhanced image using [6]; and (g) Resolution enhanced image using the proposed method.

TABLE I
SPECTRAL QUALITY METRICS FOR FIG. 2 USING DIFFERENT RESOLUTION ENHANCEMENT METHODS.

	CC	**ERGAS**	**Q4**	**RMSE**	**SAM**	**SID**
Reference values	1.0000	0.0000	1.0000	0.0000	0.0000	0.0000
Method of [1]	0.9328	6.1660	0.5988	32.5969	1.5672	0.0139
Method of [2]	0.9347	6.0853	0.6081	32.1702	1.4752	0.0137
Method of [4]	0.9796	3.4987	0.8415	18.4968	0.9468	0.0115
Method of [6]	0.9668	4.4009	0.7689	23.2654	1.0250	0.0111
Proposed method	0.9814	3.3302	0.8702	17.6056	0.8437	0.0116

calculated for different methods, and the results are shown Table I. It is clear that, the values of the metrics get closer to the optimal when using the proposed method.

In the second experiment, the resolution enhancement methods are applied twice to the LR input image as shown in Fig. 1 (c) to test their performances when the spatial resolution enhancement factor is 4 in both spatial dimensions. The subjective results are shown in Fig. 3 and the corresponding quantitative results computed using the aforementioned metrics are shown in Table II. The spectral deformations resulted from using the spatial-domain methods are apparent. Such deformations are reduced by employing the wavelet-domain methods. Furthermore, it is clear that the proposed resolution enhancement method shows better performance than that of the other methods.

We compare the computation times required by each of the image resolution enhancement methods in generating the HR image using the input LR image as shown in Fig. 1 (c) on a laptop which is operated by 32-bit Windows Vista with 2GHz Intel(R) Core(TM)2 Duo CPU, and 2GB RAM. The methods presented in this paper are implemented in MATLAB^{TM}. It takes 52, 39, 90, 4 and 10 seconds for the methods in [1], [2], [4], [6], and the proposed method, respectively, to produce the resultant HR image. The method in [4] has the highest computational cost due to its multiscale data processing, while the proposed method has a moderate computational cost.

V. CONCLUSION

A method for image resolution enhancement from a single low-resolution image using the dual-tree complex wavelet is presented. The initial rough estimate of the high-resolution image is decomposed to estimate the complex-valued high-pass wavelet coefficients for the input low-resolution image. Estimated complex wavelet coefficients are used together with the input low-resolution image to reconstruct the resultant high-resolution image by employing inverse dual-tree complex wavelet transform.

Extensive tests and comparisons with the state-of-the-art methods show the superiority of the method presented in this letter. The proposed resolution enhancement method retains both intensity and geometric features of the low-resolution image.

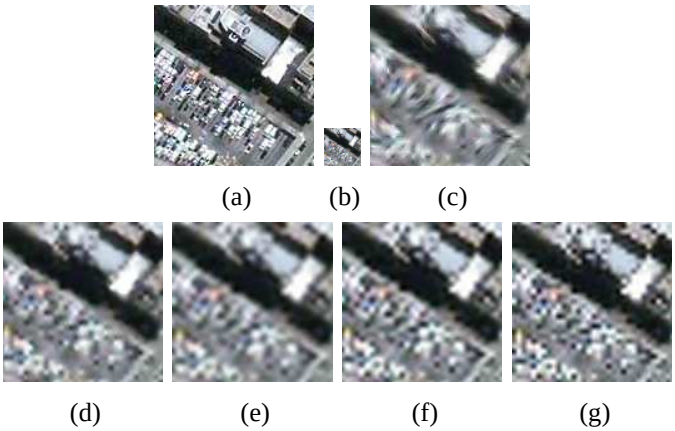

Fig. 3. Results of spatial resolution enhancement with a factor of 4 in both spatial dimensions: (a) Reference HR image; (b) Input LR image; (c) Resolution enhanced image using [1]; (d) Resolution enhanced image using [2]; (e) Resolution enhanced image using [4]; (f) Resolution enhanced image using [6]; and (g) Resolution enhanced image using the proposed method.

TABLE II
SPECTRAL QUALITY METRICS FOR FIG. 3 USING DIFFERENT RESOLUTION ENHANCEMENT METHODS.

	CC	**ERGAS**	**Q4**	**RMSE**	**SAM**	**SID**
Reference values	1.0000	0.0000	1.0000	0.0000	0.0000	0.0000
Method of [1]	0.9090	7.9112	0.4096	36.9070	1.9310	0.0125
Method of [2]	0.9085	7.8361	0.4126	37.0248	1.8312	0.0124
Method of [4]	0.9073	5.2569	0.3962	37.1817	1.8243	0.0125
Method of [6]	0.8965	6.2643	0.4024	39.4043	1.9426	0.0166
Proposed method	0.9389	4.7915	0.5615	30.8993	1.3558	0.0129

REFERENCES

[1] X. Li and M. Orchard, "New edge-directed interpolation," *IEEE Trans. Image Proc.*, vol. 10, no. 10, pp. 1521–1527, Oct 2001.

[2] L. Zhang and X. Wu, "An edge-guided image interpolation algorithm via directional filtering and data fusion," *IEEE Trans. Image Proc.*, vol. 15, no. 8, pp. 2226–2238, Aug 2006.

[3] W. K. Carey, D. B. Chuang, and S. S. Hemami, "Regularity-preserving image interpolation," *IEEE Trans. Image Proc.*, vol. 8, no. 9, pp. 1293–1297, 1999.

[4] S. Chang, Z. Cvetkovic, and M. Vetterli, "Locally adaptive wavelet-based image interpolation," *IEEE Transactions on Image Processing*, vol. 15, no. 6, pp. 1471–1485, Jun 2006.

[5] K. Kinebuchi, D. D. Muresan, and T. W. Parks, "Image interpolation using wavelet-based hidden markov trees," in *Proc. IEEE Int. Conf. Acoust. Speech and Signal Process.*, 2001, pp. 1957–1960.

[6] A. Temizel and T. Vlachos, "Wavelet domain image resolution enhancement using cycle-spinning," *Electronics Letters*, vol. 41, no. 3, pp. 119–121, Feb 2005.

[7] N. Kingsbury, "Complex wavelets for shift invariant analysis and filtering of signals," *J. Appl. Comput. Harmon. Anal.*, vol. 10, no. 3, pp. 234–253, 2001.

[8] L. Alparone, S. Baronti, A. Garzelli, and F. Nencini, "Landsat etm+ and sar image fusion based on generalized intensity modulation," *IEEE Transactions on Geoscience and Remote Sensing*, vol. 42, no. 12, pp. 2832–2839, Dec 2004.

[9] C.-I. Chang, "Spectral information divergence for hyperspectral image analysis," in *Proceedings of IEEE International Geoscience and Remote Sensing Symposium*, vol. 1, 1999, pp. 509–511.

[10] L. Alparone, S. Baronti, A. Garzelli, and F. Nencini, "A global quality measurement of pan-sharpened multispectral imagery," *IEEE Geoscience and Remote Sensing Letters*, vol. 1, no. 4, pp. 313–317, Oct 2004.

[11] L. Wald, "Quality of high resolution synthesized images: Is there a simple criterion?" in *Proceedings of International Conference on Fusion of Earth Data*, 2000, pp. 99–103.